

# External field characterization using CHAMP satellite data for induction studies

PRAVEEN KUNAGU and E CHANDRASEKHAR\*

*Department of Earth Sciences, Indian Institute of Technology Bombay, Powai, Mumbai 400 076, India.*

*\*Corresponding author. e-mail: esekhar@iitb.ac.in*

Knowledge of external inducing source field morphology is essential for precise estimation of electromagnetic (EM) induction response. A better characterization of the external source field of magnetospheric origin can be achieved by decomposing it into outer and inner magnetospheric contributions, which are best represented in Geocentric Solar Magnetospheric (GSM) and Solar Magnetic (SM) reference frames, respectively. Thus we propose a spherical harmonic (SH) model to estimate the outer magnetospheric contribution, following the iterative reweighted least squares approach, using the vector magnetic data of the CHAMP satellite. The data covers almost a complete solar cycle from July 2001 to September 2010, spanning 54,474 orbits. The SH model, developed using orbit-averaged vector magnetic data, reveals the existence of a stable outer magnetospheric contribution of about 7.39 nT. This stable field was removed from the CHAMP data after transforming to SM frame. The residual field in the SM frame acts as a primary source for induction in the Earth. The analysis of this time-series using wavelet transformation showed a dominant 27-day periodicity of the geomagnetic field. Therefore, we calculated the inductive EM  $C$ -response function in a least squares sense considering the 27-day period variation as the inducing signal. From the estimated  $C$ -response, we have determined that the global depth to the perfect substitute conductor is about 1132 km and its conductivity is around 1.05 S/m.

---

## 1. Introduction

The electrical conductivity of the subsurface can be investigated using the electromagnetic (EM) induction method, which utilizes natural magnetic field variations external to the Earth, as a primary source. The EM waves associated with these external field variations diffuse through the conducting layers of the Earth and produce eddy currents within the Earth, which in turn produce secondary magnetic fields. Thus the measurable magnetic field at the Earth's surface is the superposition of several source contributions that can be classified into external (magnetosphere, ionosphere) and internal (core, lithosphere, induced fields, etc.) parts.

Schmucker (1970) introduced the concept of perfect substitute conductor, which is a simple two-layer model with a resistive layer overlying on a high conducting layer. He devised a method to calculate the conductivity and depth estimates of a substitute conductor (the bottom layer) by estimating  $C$ -response for a permissible frequency. Since different frequencies penetrate to different depths according to skin-depth relation, which bears an inverse relation with frequency, the depth to the perfect substitute conductor differs with frequency. Figure 1 illustrates the period–depth relationship of various geomagnetic field variations, that is constrained by the skin-depth principle and thus emphasizing that, the low frequencies (periods) penetrate to deeper depths and *vice versa*.

**Keywords.** CHAMP satellite data; magnetosphere; external field characterization; EM induction response.

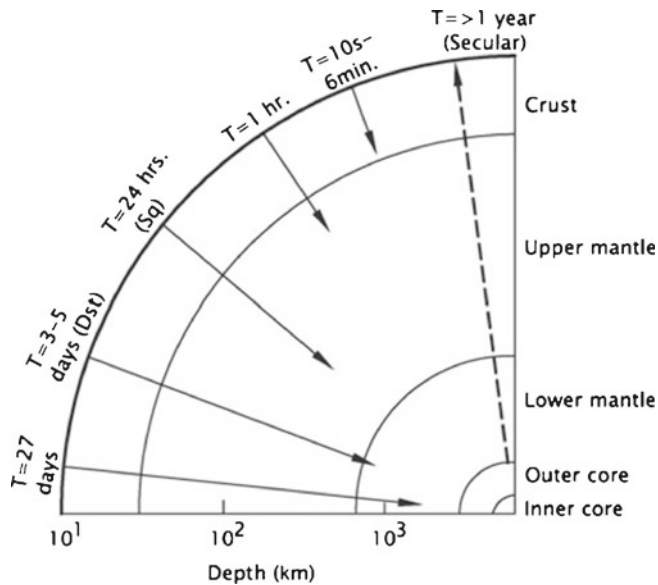


Figure 1. Sketch of various geomagnetic field variations and their penetration depths (solid arrows pointing to the center) as a function of their periodicity. The reversed dotted arrow indicates the field variations originating from the molten outer core region (after Chandrasekhar 2011).

As a result, several researchers have used a variety of geomagnetic field variations to determine the conductivity and depth estimates of the perfect substitute conductor at regional and global scales. Honkura and Matsushima (1998), Schmucker (1999), Chandrasekhar *et al.* (2003), Kuvshinov *et al.* (2007) and Everett (2010) have used Sq variations; Campbell (1990) and Chandrasekhar and Arora (1992) employed the storm-time variations; Chen and Fung (1991), Olsen (1998), Chen (2000), Chandrasekhar (2000) and Everett *et al.* (2003) have used 27-day variations, its harmonics and beyond, to estimate the depth to the perfect substitute conductor and the conductivity variations at those depth ranges.

For better estimation of induction response, knowledge of the spatial structure of the inducing field is always essential Schmucker (1985). However, for global induction studies, the sparse distribution of ground-based magnetic observatory data limits the effective characterization of inducing source. The advent of Low Earth Orbiting (LEO) satellite missions facilitate to overcome this limitation, owing to their continuous and adequate global coverage. LEO satellite missions such as MAGSAT, Ørsted and CHAMP provided valuable data with their unprecedented accuracy of measurements (Langel *et al.* 1980; Neubert *et al.* 2001; Reigber *et al.* 2002) and are helpful for a better characterization of inducing field (Olsen

1999; Constable and Constable 2004; Olsen *et al.* 2010; Everett 2010). Constable and Constable (2004) used data from the dawn-dusk orbits of MAGSAT satellite at a sampling interval of 10 s and determined the 1-D response estimates using the periodic signals ranging from Sq-variations to the annual variations. They have observed that the field components have greater power in dusk passes than the dawn passes, at all periodicities. Their results agree well with the observations of Olsen (1999) in a period band of two days to a month. Olsen *et al.* (2010) on the other hand, gave detailed insight to the concept of separation of external and internal contributions and emphasized on the use of different coordinate systems based on the geometry of the current systems of interest. Everett (2010) modelled the radial conductivity profiles of the subsurface using Sq variations and proposed a simulation scheme for extracting the Earth conductivity information from LEO satellite missions such as, CHAMP, Swarm and follow-on missions. Lesur *et al.* (2008), using first 6 years of CHAMP vector magnetometer data along with the global observatory data, had proposed an internal reference field model, GRIMM (GeoForschungsZentrum Reference Internal Magnetic Model), which describes separation between external (such as ionosphere and field aligned currents) and internal (core and lithosphere) fields. They have improved upon this model using 10 years of CHAMP and observatory data in their second version, GRIMM2 (Lesur *et al.* 2010), in which they formulated the external field to the second degree spherical harmonic using sixth order B-splines, with a knot spacing of 3 months. The knot spacing is consistent with Vector Magnetic Disturbance (VMD) index (Thomson and Lesur 2007). The VMD index can be used to monitor rapid variations in strength and direction of the large scale external field. Thus, they represent the large scale external field as a piecewise linear representation. Maus and Lühr (2005) have used Ørsted and CHAMP vector magnetic data between the years 2000 and 2004 and observed the existence of a constant magnetospheric field, confirming the earlier observations of Langel and Estes (1985a) which were based on MAGSAT data. Later using only CHAMP life-time data (2000–2010), a slight variation from their earlier findings in the magnitude of the stable magnetospheric field has been noted, with a successful identification of its source as merging electric field during the initial years (Lühr and Maus 2010). Thus the unprecedented accuracy measurements of CHAMP have been used for better characterization of external field and for more accurate resolution of several field contributions to the geomagnetic field.

In the present work, we decompose the magnetospheric contribution in long-period geomagnetic variations into outer and inner magnetospheric field contributions and estimate the respective fields by Iterative Reweighted Least Squares (IRLS) approach. We first estimate the stable outer magnetospheric field in the Geocentric Solar Magnetospheric (GSM) reference frame. This stable field is removed from the CHAMP data after rotating it into Solar Magnetic (SM) frame. The residual field in SM frame is the representative of inner

magnetospheric contribution, which is used further for the induction studies. The resultant data showed a prominent 27-day periodicity, signifying the recurrence tendency of magnetic storms, together with various other long period signals as estimated through wavelet transform (Kunagu *et al.* 2013). Accordingly, We determine the EM induction response of the Earth, for the 27-day period variation of the geomagnetic field. The organization of the paper is as follows. First we describe the data selection and processing of CHAMP satellite data following the determination of stable outer magnetospheric contribution to the geomagnetic field. Finally we determine the global induction response estimate and discuss the potential of forthcoming Swarm mission for more reliable and accurate geomagnetic field modelling.

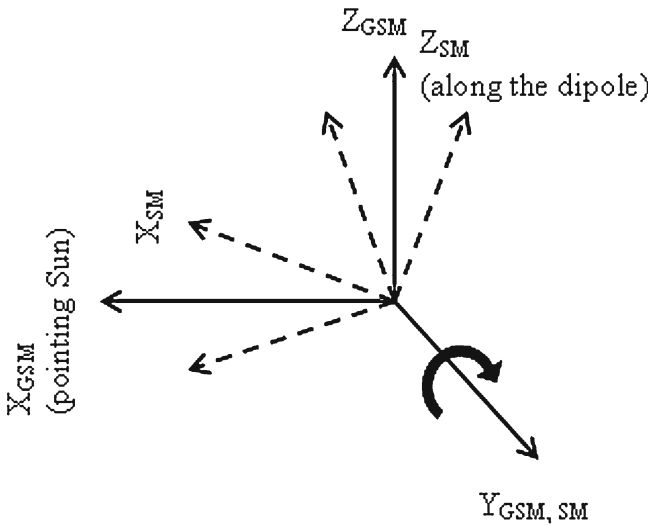


Figure 2. Orientation of field vectors in geocentric solar magnetospheric and solar magnetic reference frames.

## 2. Data selection and processing

Raw CHAMP vector magnetometer data of 1-sec sampling interval, spanning from 2001.0 to 2010.7 comprising of 55,417 tracks corresponding to nighttime (1800 to 0600 LT; LT = UT + longitude/15) were obtained. After visual inspection of the data for jumps, missing values, etc., and after removing such spurious data, a total of 54,474 tracks only were finally considered for further analysis. The broad LT window led to a larger data volume and ensured full night-time coverage and was helpful in

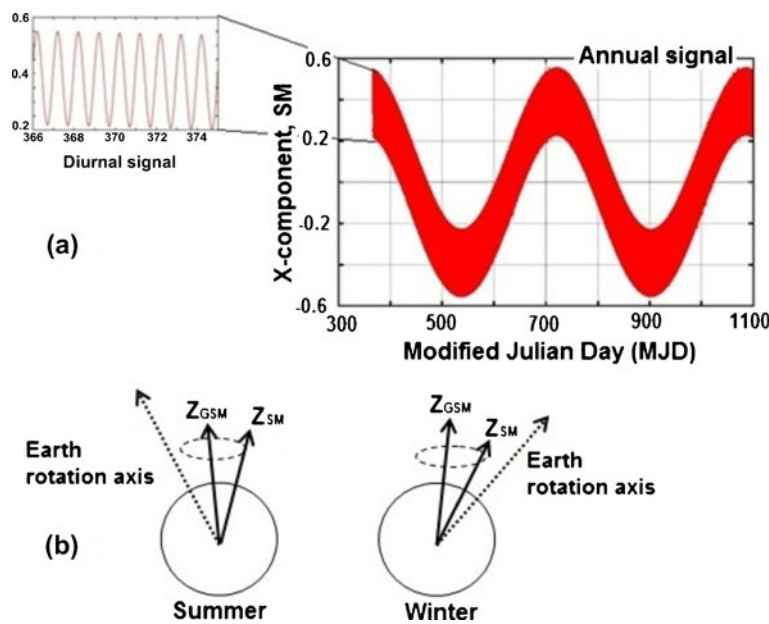


Figure 3. Rotational transformation from GSM to SM frame. (a) Diurnal and annual signals along  $X_{SM}$  after transforming a constant field (synthetic) along  $Z_{GSM}$  with unit value, i.e.,  $B_{x_{GSM}} = 0$ ,  $B_{y_{GSM}} = 0$  and  $B_{z_{GSM}} = 1$  nT. (b) Pictorial representation of how the revolution of  $Z_{SM}$  around  $Z_{GSM}$  and with respect to Earth rotation axis, produces daily and annual signals. The small dotted circle represents the daily variation and  $Z_{SM}$  makes one revolution about  $Z_{GSM}$  in 365 days, which is the annual variation.

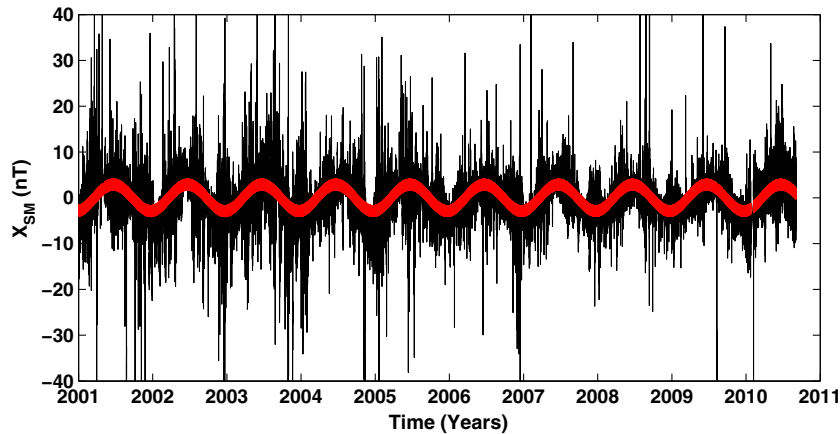


Figure 4. Orbit-averages of CHAMP field residuals along X-direction in SM frame (after removing core and lithospheric fields). The red line is the stable Z-GSM field after rotating it into the SM frame (see text for more information).

identifying the LT dependencies of the field variations if any. Night-time data are chosen to reduce the ionospheric effects in the data. To minimize the effect of high latitude auroral electrojet and field aligned currents, data confined to mid-latitudes ( $\pm 50^\circ$  geomagnetic latitude) were selected. Since the stable outer magnetospheric field exists irrespective of the type of the day (disturbed or quiet), no activity-based selection criteria was imposed on the data. Further to obtain the external field variations, the slowly varying core field (up to SH degree 14) and the lithospheric field (up to SH degree 60) are removed using GRIMM2 (Lesur *et al.* 2010).

Maus and Lühr (2005) proposed that, the outer and inner magnetospheric contributions can be best represented in GSM and SM reference frames, respectively. Figure 2 shows the orientation of field vectors in these two reference frames. The transformation from GSM to SM (*vice versa*) is simply a rotation about the Y-axis by the dipole tilt angle, projected onto the plane containing both the dipole axis and the Sun-Earth line. In principle, a stable field in GSM transforms to a periodic signal having diurnal and annual variations, when rotated into SM frame. Figure 3(a) shows such a periodic signal in SM frame, when a stable field of arbitrary amplitude along Z-GSM is rotated to the SM frame. Figure 3(b) depicts the daily and seasonal wise rotational transformation of the field vectors, which is responsible for the diurnal and annual signals.

Traditionally the time series of the field components designate the hourly averages. However, due to inconsistency in the availability of uniform hourly averages along each orbit, orbit averages of the field values have been considered in the present study. The orbit averages are the averages of field values along the CHAMP passes (pole to pole traverse) in the night side region. Such an

averaging also minimizes the influence of residual lithospheric signals and localized perturbations of the magnetic field. Figure 4 shows the orbit averages of CHAMP residuals (after removing the core and lithospheric fields) in SM frame along X-direction. The orbit averages are less noisy and dominant periodicities in the field residuals are clearly visible. Figure 4 shows the periodic signal (red curve) that was obtained after transforming the stable field in GSM frame into the SM frame and when superimposed on the orbit averaged data (black lines), it exactly matches with the annual signal present in the data.

### 3. Methodology and results

The internal ( $V_i$ ) and external ( $V_e$ ) parts of the geomagnetic potential  $V(r, \theta, \phi, t)$  in terms of a series of spherical harmonics is expressed as:

$$\begin{aligned}
 V_i(r, \theta, \phi, t) &= a \sum_{l=1}^L \sum_{m=0}^l [g_l^m(t) \cos m\phi + h_l^m(t) \sin m\phi] \\
 &\quad \times \left(\frac{a}{r}\right)^{l+1} P_l^m(\cos \theta) \quad (1)
 \end{aligned}$$

$$\begin{aligned}
 V_e(r, \theta, \phi, t) &= a \sum_{l=1}^L \sum_{m=0}^l [q_l^m(t) \cos m\phi + s_l^m(t) \sin m\phi] \\
 &\quad \times \left(\frac{r}{a}\right)^l P_l^m(\cos \theta) \quad (2)
 \end{aligned}$$

where,  $\theta$ ,  $\phi$ ,  $r$  and  $t$  stand for geocentric colatitude, longitude, radius (distance to the observation point from the center of Earth) and time;  $a = 6371.2$  km

being the Earth radius.  $P_l^m$  are Schmidt quasi normalized spherical harmonic (SH) functions.  $(g_l^m, h_l^m)$  and  $(q_l^m, s_l^m)$  are internal and external Gauss coefficients, respectively, with degree  $l$ , order  $m$  and  $L$  being the truncation factor.

Lesur *et al.* (2008) gave expressions for magnetic field components of internal origin and for only Z-component for external sources. Here we present expressions for all the three vector directions of both internal and external origin in geocentric Cartesian reference frame (equations 3–8). These are generalized equations which are valid for the geocentric Cartesian reference frames such as, GSM, SM and geographic coordinates (GEO) and are derived using the recurrence relations for the quasi-normalized functions,  $P_l^m$  (Backus *et al.* 1996). For other coordinate systems, the respective transformation matrices should be employed.

The magnetic field components derived from the scalar potential of internal and external origin (equations 1 and 2, respectively) along the X-, Y- and Z-directions can be written as:

Internal:

$$\begin{aligned}
 B_x^i = & - \sum_{l=1}^L \sum_{m=0}^l \frac{1}{2} \left(\frac{a}{r}\right)^{l+2} \\
 & \times \{ \sqrt{(l+m+1)(l+m+2)} \\
 & \times [g_l^m \cos(m+1)\phi + h_l^m \sin(m+1)\phi] \\
 & \times P_{l+1}^{m+1}(\cos\theta) \\
 & - \sqrt{(l-m+1)(l-m+2)} \\
 & \times [(g_l^m \cos(m-1)\phi + h_l^m \sin(m-1)\phi) \\
 & \times P_{l+1}^{m-1}(\cos\theta)] \} \quad (3)
 \end{aligned}$$

$$\begin{aligned}
 B_y^i = & - \sum_{l=1}^L \sum_{m=0}^l \frac{1}{2} \left(\frac{a}{r}\right)^{l+2} \\
 & \times \{ \sqrt{(l+m+1)(l+m+2)} \\
 & \times [g_l^m \sin(m+1)\phi - h_l^m \cos(m+1)\phi] \\
 & \times P_{l+1}^{m+1}(\cos\theta) \\
 & + \sqrt{(l-m+1)(l-m+2)} \\
 & \times [g_l^m \sin(m-1)\phi - h_l^m \cos(m-1)\phi] \\
 & \times P_{l+1}^{m-1}(\cos\theta) \} \quad (4)
 \end{aligned}$$

and

$$\begin{aligned}
 B_z^i = & \sum_{l=1}^L \sum_{m=0}^l \left(\frac{a}{r}\right)^{l+2} \sqrt{(l+m+1)(l-m+1)} \\
 & \times [g_l^m \cos m\phi + h_l^m \sin m\phi] P_{l+1}^m(\cos\theta). \quad (5)
 \end{aligned}$$

External:

$$\begin{aligned}
 B_x^e = & \frac{1}{\sqrt{2}} \sum_{l=1}^L \sum_{m=0}^l \left(\frac{r}{a}\right)^{l-1} \\
 & \times \{ \sqrt{(l+m)(l+m-1)} \\
 & \times [q_l^m \cos(m-1)\phi + s_l^m \sin(m-1)\phi] \\
 & \times P_{l-1}^{m-1}(\cos\theta) \\
 & - \sqrt{(l-m)(l-m-1)} \\
 & \times [q_l^m \cos(m+1)\phi + s_l^m \sin(m+1)\phi] \\
 & \times P_{l-1}^{m+1}(\cos\theta) \} \quad (6)
 \end{aligned}$$

$$\begin{aligned}
 B_y^e = & \frac{1}{\sqrt{2}} \sum_{l=1}^L \sum_{m=0}^l \left(\frac{r}{a}\right)^{l-1} \\
 & \times \{ \sqrt{(l+m)(l+m-1)} \\
 & \times [s_l^m \cos(m-1)\phi - q_l^m \sin(m-1)\phi] \\
 & \times P_{l-1}^{m-1}(\cos\theta) \\
 & + \sqrt{(l-m)(l-m-1)} \\
 & \times [s_l^m \cos(m+1)\phi - q_l^m \sin(m+1)\phi] \\
 & \times P_{l-1}^{m+1}(\cos\theta) \} \quad (7)
 \end{aligned}$$

and

$$\begin{aligned}
 B_z^e = & - \sum_{l=1}^L \sum_{m=0}^l \left(\frac{r}{a}\right)^{l-1} \sqrt{(l-m)(l+m)} \\
 & \times [q_l^m \cos m\phi + s_l^m \sin m\phi] P_{l-1}^m(\cos\theta). \quad (8)
 \end{aligned}$$

The  $l = 1$  and  $m = 0$  term in equations (6–8), corresponds to the large-scale external magnetic field of magnetospheric origin and is constant along the three vector directions. These first-degree terms can be used to represent most of the large-scale stable external fields (Velínský *et al.* 2006).

### 3.1 Estimation of outer and inner magnetospheric contributions through iterative reweighted least squares (IRLS) approach

For effective characterization of the source field for induction purpose, the field contributions from outer and inner magnetosphere need to be separated. In particular for the present study, the inner magnetospheric contribution is of special interest, which acts as primary source for the induction phenomenon to occur inside the Earth. The determination of these field contributions is carried out using IRLS technique (Farquharson and

Oldenburgh 1998). This approach facilitates to overcome the complexity in using the traditional  $L_2$  norm solution (Farquharson and Oldenburgh 1998).

The IRLS technique is a simple but effective iterative algorithm which in fact starts with  $L_2$  norm solution of the forward problem

$$\mathbf{d} = \mathbf{G}\mathbf{m} \quad (9)$$

and solves a sequence of weighted least squares equations whose solution converges to  $L_1$  norm minimizing solution.

In equation (9),  $\mathbf{d}$  represents the data,  $\mathbf{G}$  is the kernel matrix having the spatial distribution of data points along each orbit of CHAMP that are determined from equations (6–8) and  $\mathbf{m}$  denotes the model parameters.

Now we need to minimize the residual vector  $\mathbf{r} = \mathbf{d} - \mathbf{G}\mathbf{m}$ , i.e.,

$$f(\mathbf{m}) = \|\mathbf{r}\|_1 = \sum_{i=1}^m |r_i|. \quad (10)$$

The derivative of  $f$  is

$$\frac{\partial f(\mathbf{m})}{\partial m_k} = \sum_{i=1}^m G_{i,k} \frac{1}{|r_i|} r_i \quad (11)$$

and the gradient of  $f$  can be written as:

$$\nabla f(\mathbf{m}) = \mathbf{G}^T \mathbf{R} \mathbf{r} = \mathbf{G}^T \mathbf{R} (\mathbf{d} - \mathbf{G}\mathbf{m}) \quad (12)$$

where  $\mathbf{R}$  is the diagonal weighting matrix ( $R_{i,i} = 1/|r_i|$ ).

To find the  $L_1$  norm minimizing solution we solve  $\nabla f(\mathbf{m}) = \mathbf{0}$ , which gives

$$\mathbf{G}^T \mathbf{R} \mathbf{d} = \mathbf{G}^T \mathbf{R} \mathbf{G} \mathbf{m}. \quad (13)$$

Thus, the algorithm begins with the  $L_2$  norm solution  $\mathbf{m}^0 = \mathbf{m}_{L_2}$  and by determining the appropriate weighting matrix,  $\mathbf{R}$ , we calculate the corresponding residual vector  $\mathbf{r}^0 = \mathbf{d} - \mathbf{G}\mathbf{m}^0$ . Now equation (13), can then be solved to obtain a new model  $\mathbf{m}^1$  and associated residual vector  $\mathbf{r}^1$ . The process is repeated until the model ( $\mathbf{m}^n - \mathbf{m}^{n-1}$ ) and residual ( $\mathbf{r}^n - \mathbf{r}^{n-1}$ ) vectors converge, where  $n$  denotes the number of iterations.

### 3.1.1 Estimation of stable outer magnetospheric contribution

The stable field of outer magnetospheric origin is estimated using a single Gauss coefficient of degree 1 and order 0 along Z-direction in GSM frame ( $q_1^{0GSM}$ ), using the average of 10 years (3650 days)

of CHAMP data. Lühr and Maus (2010) observed that the stable GSM field is caused by tail currents and shows no solar cycle dependency. Thus, the choice of a single Gauss coefficient in the present study to estimate the stable outer magnetospheric field can be justified.

### 3.1.2 Estimation of inner magnetospheric contribution

In order to examine the time evolution of the inner magnetospheric field, 10 years (3650 days) of CHAMP data was sampled at 100 days interval. This gives a total of 36 coefficients corresponding to degree 1 and order 0 along Z-direction ( $q_1^{0SM}$ ) and another set of 36 coefficients corresponding to degree 1 and order 1 along X-direction ( $q_1^{1SM}$ ) in SM frame.

Thus, we model the stable outer magnetospheric field with one Gauss coefficient along Z-GSM and the inner magnetospheric field using 72 Gauss coefficients along Z-SM and X-SM directions, totaling to 73 coefficients.

Now, we fit the data by adjusting the Gauss coefficients, that is carried out following the IRLS technique using  $L_1$  norm minimizing solution as described above. It is observed that, the residual vector (equation 10) converges after 60 iterations and the large-scale external stable field in GSM ( $Z_{GSM}$ ) is estimated to be  $7.39 \pm 0.11$  nT. Figure 5 shows the final estimated model parameters with their standard deviations, indicating the robustness of estimating these parameters. The magnetospheric field aligned with the  $Z_{SM}$  component shows pronounced solar cycle dependence, with high energy during initial years (corresponding to the parameters 2 to 18) and decline in energy during solar low period (parameters 19 to 36), whereas,  $X_{SM}$  has no influence of solar cycle.

It is important to note here that, a strict separation of both outer and inner magnetospheric contributions is not possible. However, we believe that, these field contributions can be best represented in GSM and SM reference frames.

Finally, we prepare a time series in SM frame by subtracting the stable GSM field contribution from the CHAMP data. As a result, the final residual time series contains contribution only from magnetospheric ring-current and its induced counterpart. The ratio of induced to inducing field components as a function of frequency, gives the induction response.

### 3.2 Estimation of induction response

The residual time series, which is obtained after removing the stable outer-magnetospheric field

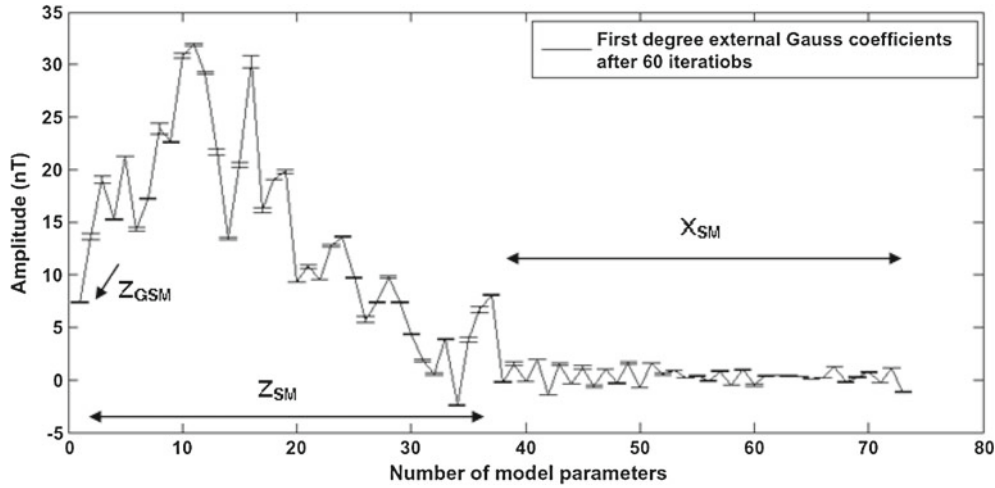


Figure 5. Spherical harmonic model parameters,  $Z_{GSM}$ ,  $Z_{SM}$  and  $X_{SM}$  determined using  $L_1$  norm (after 60 iterations) using CHAMP orbit-averaged data between the years 2001 and 2010.

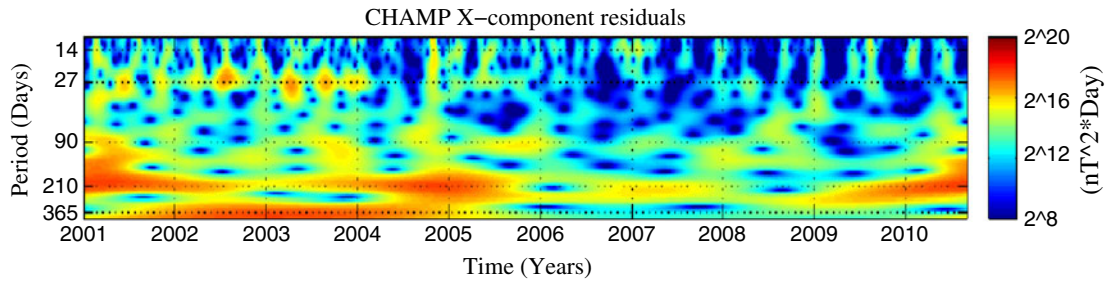


Figure 6. Wavelet power spectrum of CHAMP X-residuals showing the geomagnetic periodic signals and their time evolution. The 27-day periodicity is shown as intermittent temporal structure.

from the CHAMP data, contains contributions only from inner-magnetosphere (i.e., ring-current) and its induced counterpart. Thus the ratio of vertical (induced) to horizontal (inducing) components as a function of frequency, gives us the depth to the perfect substitute conductor (Schmucker 1970).

The long wavelength analysis of geomagnetic field using CHAMP time-series through wavelet transform in SM frame, showed the dominant 27-day periodicity existing irrespective of the type of the day (disturbed or quiet) (Kunagu *et al.* 2013). Figure 6 shows the 27-day periodic signal in the wavelet power spectrum of CHAMP X-residuals, which is observed as an intermittent temporal structure.

Now, the induction response is determined with  $C(\omega)$  as transfer function, where  $\omega = 0.037$  cycles/day, that corresponds to the 27-day period variations of the geomagnetic field.

Therefore,

$$Z(\omega) = C(\omega) \cdot H(\omega). \quad (14)$$

The least squares solution for  $C(\omega)$  is given by

$$C(\omega) = \sum^N Z(\omega) \cdot H^*(\omega) / \sum^N H(\omega) \cdot H^*(\omega) \quad (15)$$

where  $*$  denotes the complex conjugate and  $N$  denotes the number of samples.

Thus the estimated complex  $C$ -response for the 27-day period variation is

$$C(\omega) = 1131.5718 - 375.1946i. \quad (16)$$

The real part of the  $C$ -response ( $\text{Re } C(\omega)$ ) gives the depth of penetration of the induced currents and the imaginary part ( $\text{Im } C(\omega)$ ) is used to

determine the conductivity ( $\sigma$ ) of the substitute conductor at that depth. The conductivity can be estimated by Chen and Fung (1991)

$$\sigma = 0.253 \cdot 86400 \cdot T/4(C_{\text{imag}})^2 = 1.05 \text{ S/m} \quad (17)$$

where  $T$  is the periodicity of the inducing signal in units of days and  $\sigma$  is in units of S/m.

The estimated global induction response, corresponding depth to the conductosphere and conductivity value are compatible with the earlier observations. For example, using MAGSAT data (Langel 1990; Everett *et al.* 2003; Constable and Constable 2004); using a chain of land-based observatories: for storm-time period data (Chandrasekhar and Arora 1992) and for 27-day period variations and its harmonics Chandrasekhar (2000); using Ørsted satellite data (Olsen 1999); using CHAMP data (Velínský *et al.* 2006). Table 1 shows a comparison between the estimated conductosphere depth and the conductivity value in the present study and the earlier observations.

#### 4. Discussion

Using MAGSAT data, Langel and Estes (1985a) estimated the total magnetospheric field contribution to be about 20 nT. Maus and Lühr (2005) using first five years of Ørsted and CHAMP satellite data, estimated the contribution of outer magnetospheric field to be around 13 nT in GSM frame. They have modelled this field by expanding the spherical harmonics up to the second degree, following a linear least squares fit to the satellite data. Later, Lühr and Maus (2010) in their recent study, using 10 years of CHAMP data, carried out similar analysis and estimated the outer magnetospheric contribution to be around 8.31 nT in GSM frame. In the present study, the stable

GSM field estimated using IRLS technique is 7.39 nT. A careful observation of all the GSM values estimated by several workers clearly explain that, differences between successive estimates have gradually decreased. The steady progress in this direction could be best attributed to the processing and statistical techniques developed. Thus, the stable GSM field of 7.39 nT that we have obtained in this study is more robust as it was estimated following IRLS approach using  $L_1$  norm, which is less sensitive to the outliers present in the data.

However, we emphasize here that, the magnetospheric field has complex morphology and it is quite possible that the other current systems present in the magnetosphere, such as cusp currents, high- and low-latitude oval currents, etc., may give such discrepancies in the estimated values. Nakano *et al.* (2002); Nakano and Iyemori (2003) also suggest that the inter-hemispheric currents, triggered by an imbalance between the polar electric fields which are known to be strongly influenced by IMF By component also cannot be neglected. Further, the directional dependence of the solar cycle influence on the geomagnetic field (figure 5) indicates the necessity for better understanding of the Sun–Earth interaction and design of highly complex mathematical algorithms.

Such a precise characterization of the external source field has facilitated us to have more confidence on the estimated induction response. The depth to the perfect substitute conductor and its conductivity reported in the present study are in good agreement with the earlier estimated regional and global estimates (table 1).

Chandrasekhar (2000) employing the complex demodulation technique and considering only those demodulates, which satisfy the  $P_1^0$  characteristic of the inducing source field, estimated the depth of the conductosphere to be 1200 km with an average conductivity of 0.7 S/m. As observed by Olsen (1998), the EM response obtained by the combined analysis of Sq and geomagnetic storm-time

Table 1. Comparison of estimates of depth to the conductosphere and the conductivity value of the present study with the earlier observations.

Previous works	Depth to the conductosphere (km)	Conductivity value (S/m)
Langel (1990)	1138	–
Olsen (1998)	>800	1.7
Chandrasekhar (2000)	1200	0.7
Everett <i>et al.</i> (2003)	>670	1.0
Utada <i>et al.</i> (2003)	>850	1.6
Constable and Constable (2004)	1300	–
Velínský <i>et al.</i> (2006)	>1300	6
Kuvshinov and Olsen (2006)	900	1 to 2
Present work	1132	1.05

variations for European region also shows a well-marked conductivity increase at around 800 km depth. Constable and Constable (2004) observed an increase in conductivity from 0.01 to about 2 S/m at a depth of around 700 km (associated with the 660 km seismic discontinuity) and a further increase in conductivity is also been observed at a depth of about 1300 km, the top of the lower mantle. Velínský *et al.* (2006) using the CHAMP vector magnetometer data corresponding to the storm-time variations, derived the time-domain electrical conductivity structure of the Earth's mantle. They could identify the conductivity jump at 660 km seismic discontinuity and estimated the upper and lower mantle conductivities to be around 0.01 and 6 S/m, respectively.

## 5. Conclusion

We have presented a simple SH model in GSM frame, characterizing the outer magnetospheric contribution, following an iterative reweighted least squares approach using  $L_1$  norm and identified the existence of a stable field with a magnitude of about 7.39 nT. For the purpose of induction studies, this stable field whose source is located in the magnetospheric tail currents, can be considered as far field and was removed from the CHAMP data after transforming to SM frame. The response of the Earth to the external time varying signal with 27-day periodicity is estimated through the  $C$ -response and the determined average global conductosphere depth of about 1132 km and the conductivity estimation of 1.05 S/m, are in agreement with the earlier observations.

Further high precision data from the much awaited 3-satellite Swarm mission of European Space Agency, which is scheduled to be launched in 2013 is expected to improve the spatial and temporal variations of the geomagnetic field efficiently, as the magnetic field measurements will be made simultaneously at different altitudes and local times. However, since the fields measured by observatories and satellites are different because of the altitude difference and the frame of reference in which they record the field variations, the joint analysis of satellite and observatory data could yield promising results for a better knowledge of the factors contributing/influencing the geomagnetic field and their evolution, due to their spatio-temporal distribution and the area of influence.

## Acknowledgements

The authors thank the CHAMP data processing team at GFZ for providing fully calibrated

vector magnetometer data. The support from Prof. Mioara Mandea is greatly acknowledged. PK acknowledges Vincent Lesur for helpful discussions and explanation of GRIMM2 algorithm. This work is funded by Deutscher Akademischer Austausch Dienst (DAAD) and partly by ISRO-PLANEX, Physical Research Laboratory (PRL), India.

## References

- Backus G, Parker R and Constable C 1996 *Foundations of Geomagnetism* (New York: Cambridge University Press), 369p.
- Campbell W H 1990 The magnetospheric disturbance ring current as a source for probing the deep earth electrical conductivity; *Pure Appl. Geophys.* **134** 541–557.
- Chandrasekhar E 2000 Geo-electrical structure of the mantle beneath the Indian region derived from the 27-day variation and its harmonics; *Earth Planets Space* **52** 587–594.
- Chandrasekhar E 2011 Regional electromagnetic induction studies using long period geomagnetic variations; In: *The earth's magnetic interior* (eds) Petrovský E, Herrero-Bervera E, Harinarayana T and Ivers D; *IAGA Special Sopron Book Series, Springer* **1** 31–42.
- Chandrasekhar E and Arora B R 1992 Upper mantle electrical conductivity distribution beneath the Indian sub-continent using geomagnetic storm time variations; *Geol. Soc. India Memoir* **24** 149–157.
- Chandrasekhar E, Oshiman N and Yumoto K 2003 On the role of oceans in the geomagnetic induction by Sq along the 210 deg magnetic meridian region; *Earth Planets Space* **55** 315–326.
- Chen P F 2000 Electromagnetic response function for the semi-annual variations estimated by the single-station method using the night-time values of the geomagnetic fields; *Acta Seismol. Sinica* **13**(3) 316–324.
- Chen P F and Fung P C W 1991 Electromagnetic response function for the period of 27-day in the Chinese region; *J. Geomag. Geoelectr.* **43** 978–987.
- Constable S and Constable C 2004 Observing geomagnetic induction in magnetic satellite measurements and associated implications for mantle conductivity; *Geochem. Geophys. Geosys.* **5** Q01006.
- Everett M E 2010 Spatiotemporal sampling of Sq+-induced geomagnetic responses at LEO satellite altitude for a radially conductive Earth; *Geophys. J. Int.* **183** 1185–1198.
- Everett M, Constable S and Constable C 2003 Effects of near-surface conductance on global satellite induction responses; *Geophys. J. Int.* **153** 277–286.
- Farquharson C and Oldenburgh D 1998 Non-linear inversion using general measures of data misfit and model structure; *Geophys. J. Int.* **134** 213–227.
- Honkura Y and Matsushima M 1998 Electromagnetic response of the mantle to long-period geomagnetic variations over the globe; *Earth Planets Space* **50** 651–662.
- Kunagu P, Balasis G, Lesur V, Chandrasekhar E and Papadimitriou C 2013 Wavelet characterization of external magnetic sources as observed by CHAMP satellite: Evidence for unmodelled signals in geomagnetic field models; *Geophys. J. Int.* **192**(3) 946–950, doi: [10.1093/gji/ggs093](https://doi.org/10.1093/gji/ggs093).
- Kuvshinov A and Olsen N 2006 A global model of mantle conductivity derived from 5 years of CHAMP, Ørsted

- and SAC-C magnetic data; *Geophys. Res. Lett.* **33** doi: [10.1029/2006GL027083](https://doi.org/10.1029/2006GL027083).
- Kuvshinov A, Manoj C, Olsen N and Sabaka T 2007 On induction effects of geomagnetic daily variations from equatorial electrojet and solar quiet sources at low and middle latitudes; *J. Geophys. Res. (Solid Earth)* **112** 10,102.
- Langel R A 1990 Study of the crust and mantle using magnetic surveys by Magsat and other satellites; *Proc. Indian Acad. Sci. (Earth Planet. Sci.)* **99(4)** 581–618.
- Langel R A and Estes R H 1985a Large-scale, near-Earth magnetic fields from external sources and the corresponding induced internal field; *J. Geophys. Res.* **90** 2487–2494.
- Langel R A, Estes R H, Mead G D, Fabiano E B and Lancaster E R 1980 Initial geomagnetic field model from MAGSAT vector data; *Geophys. Res. Lett.* **7** 793–796.
- Lesur V, Wardinski I, Hamoudi M and Rother M 2010 The second generation of the GFZ reference internal magnetic model: GRIMM-2; *Earth Planets Space* **62** 765–773.
- Lesur V, Wardinski I, Rother M and Mandea M 2008 GRIMM – The GFZ reference internal magnetic model based on vector satellite and observatory data; *Geophys. J. Int.* **173** 382–394.
- Lühr H and Maus S 2010 Solar cycle dependence of quiet-time magnetospheric currents and a model of their near-Earth magnetic fields; *Earth Planets Space* **62** 843–848.
- Maus S and Lühr H 2005 Signature of the quiet-time magnetospheric magnetic field and its electromagnetic induction in the rotating earth; *Geophys. J. Int.* **162** 755–763.
- Nakano S and Iyemori T 2003 Local time distribution of net field-aligned currents derived from high-altitude satellite data; *J. Geophys. Res. (Space Physics)* **108** 1314.
- Nakano S, Iyemori T and Yamashita S 2002 Net field-aligned currents controlled by the polar ionospheric conductivity; *J. Geophys. Res. (Space Physics)* **107** 1056.
- Neubert T, Mandea M, Hulot G, von Freese R, Primdahl F, Jørgensen J, Friis-Christensen E, Stauning P, Olsen N and Risbo T 2001 Ørsted satellite captures high-precision geomagnetic field data; *EOS Trans. AGU* **82(7)** 81–88.
- Olsen N 1998 The electrical conductivity of the mantle beneath Europe derived from *C*-responses from 3 to 720 hr; *Geophys. J. Int.* **133** 298–308.
- Olsen N 1999 Long-period (30 days–1 year) electromagnetic sounding and the electrical conductivity of the lower mantle beneath Europe; *Geophys. J. Int.* **138** 179–187.
- Olsen N, Glassmeier K H and Jia X 2010 Separation of the magnetic field into external and internal parts; *Space Sci. Rev.* **152** 135–157.
- Reigber C, Lühr H and Schwintzer P 2002 CHAMP mission status; *Adv. Space Res.* **30(2)** 129–134.
- Schmucker U 1970 *Anomalies of geomagnetic variations in the southwestern United States*; University of California Press, Berkeley.
- Schmucker U 1985 Magnetic and electric fields due to electromagnetic induction by external sources, Electrical Properties of the Earth's Interior; *New Series Group V Springer-Verlag* **2b** 100–125.
- Schmucker U 1999 A spherical harmonic analysis of solar daily variations in the years 1964–1965: Response estimates and source fields for global induction – II. Results; *Geophys. J. Int.* **136** 455–476.
- Thomson A W P and Lesur V 2007 An improved geomagnetic data selection algorithm for global geomagnetic field modelling; *Geophys. J. Int.* **169** 951–963.
- Utada H, Koyama T, Shimizu H and Chave A D 2003 A semi-global reference model for electrical conductivity in the mid-mantle beneath the north Pacific region; *Geophys. Res. Lett.* **30(4)** 1994, doi: [10.1029/2002GL016092](https://doi.org/10.1029/2002GL016092).
- Velínský J, Martinec Z and Everett M E 2006 Electrical conductivity in the Earth's mantle inferred from CHAMP satellite measurements – I. Data processing and 1-D inversion; *Geophys. J. Int.* **166** 529–542.